On the Behavior of Surface Plasmons at a Metallo-Dielectric Interface

Robert D. Nevels, *Life Fellow, IEEE*, and Krzysztof A. Michalski, *Fellow, IEEE*

***Abstract*—In an attempt to shed additional light on the extraordinary transmission of an electromagnetic wave through a sub-wavelength aperture, we undertake a more detailed analysis of the canonical problem of the magnetic field of a line source located at a silver–dielectric interface at optical wavelengths. In particular, we present a closed-form asymptotic evaluation of the branch cut integral and show that the branch cut term initially decays as $x^{-1/2}$, where x is the distance between the source and the field point along the interface, but for larger distances, it falls off more rapidly as $x^{-3/2}$. We also address the effect on a surface plasmon of a tarnished silver substrate. Our analysis supports the extraordinary transmission surface plasmon electromagnetic interaction model, explains the origin of the so-called "creeping wave," and shows that the tarnish layer has a significant damping effect on the surface plasmon polariton.**

***Index Terms*—Extra ordinary transmission, lateral wave, plasmons, Sommerfeld integral, space wave, Zenneck wave.**

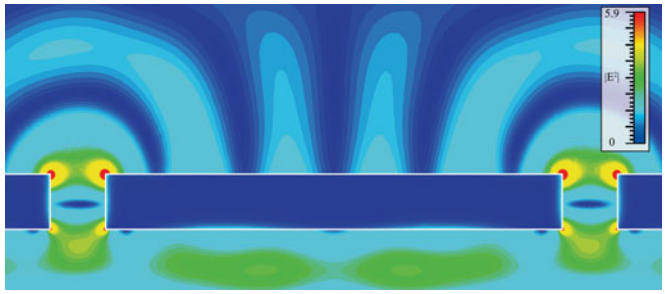

Fig. 1. Numerical calculation (CST©) showing a surface plasmon standing wave E^2 pattern on a thin silver plate with dielectric constant $\varepsilon_r = -18.242 + j1.195$ between two slots illuminated by a 660 nm plane wave from below. The center plate has a length $5/2\lambda_{\rm spp}$ (1650 nm) and each aperture has a width and thickness of $\lambda_{\rm spp}/3$(200 nm).

I. Introduction

THE report in 1998 [1] of radically enhanced transmission through arrays of sub-wavelength holes in thin metal films, a phenomenon known as extraordinary optical transmission (EOT), has spurred an explosion of interest in the mechanisms involved in the electromagnetic interaction between optical nano-objects, at metallo-dielectric interfaces. In classical electromagnetics, the Bethe [2] and Bouwkamp [3], [4] theory tells us that the power transmitted through an aperture in an infinitely thin metallic screen scales as the inverse fourth power of the aperture size in terms of wavelengths. Very little power is transmitted through a sub-wavelength aperture in a thin, perfect conducting screen. If the screen is made to be of finite thickness, then an additional reduction in the transmitted field strength will result, due the below-cutoff dimensions of the slot. However, it was discovered – first experimentally and then confirmed by numerical analysis, as shown in Fig. 1 – that for metals at optical frequencies there are situations where remarkable amounts of energy pass through sub-wavelength slits and holes.

To illustrate, Fig. 1 shows a cross-sectional view of a metallic sheet made of silver with two slots passing through the sheet. This nanostructure is excited by a plane wave from below. The magnitude of the field intensity shows a complicated structure with significant field at the slot corners, an interaction resulting in strong standing waves in the horizontal direction below, some weak field transmission through the slots, and a standing wave pattern on top of the center plate.

Ebbesen *et al.* [1] explained EOT in terms of surface plasmon polaritons (SPP), a cloud of unattached electrons moving through a lattice of stationary ions. For many metals at near-infrared and optical frequencies, the real part of the dielectric constant is negative, consistent with the properties of a plasma below the plasma frequency. Going back to Fig. 1, the prevailing view is that a plasmon resonance occurs at the bottom aperture, where high field points are seen to occur at the interior corners of the slot enhancing the field amplitude by several orders of magnitude. Even though the field experiences attenuation as it passes through the slot, the total power emerging is greater than the power incident on the slot apertures from below.

Recently, Lezec and Thio [5] published an alternative scalar diffraction theory, according to which SPPs are not responsible for the enhanced transmission through the sub-wavelength holes. This theory predicts a damping factor of $1/x$ in the field, where x is the distance from a perturbation or aperture along the interface. However, a scalar analysis does not account for polarization effects in electromagnetics and transverse electric (TE) and transverse magnetic (TM) waves behave differently. Nonetheless their theory was accompanied by experiment performed on a silver bar by Gay *et al.* [6], which fit the predicted $1/x$ decay rate.

The Lezec and Thio [5] theory was questioned by Lalanne and Hugonin [7], who conjectured that the coupling mechanism is due to a SPP interacting with what they refer to as a creeping wave that has a damping factor $x^{-1/2}$. A SPP has an exponential decay factor, however the loss is comparably small, allowing

Manuscript received May 4, 2014; revised June 28, 2014 and July 13, 2014; accepted July 15, 2014. Date of publication July 24, 2014; date of current version August 27, 2014.

The authors are with the Department of Electrical and Computer Engineering, Texas A&M University, College Station, TX 77843 USA (e-mail: nevels@ece.tamu.edu; krys@ece.tamu.edu).

Color versions of one or more of the figures in this paper are available online at http: // ieeexplore.ieee.org.

Digital Object Identifier 10.1109/JLT.2014.2343018

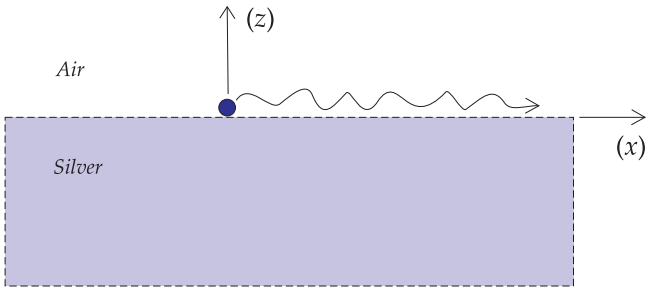

Fig. 2. A magnetic line source placed at the origin on the interface between silver and air half-spaces.

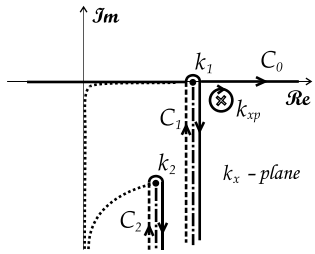

Fig. 3. Complex plane integration path around branch cuts connecting the branch points k1 and k2, the wave numbers for air and silver respectively, and the SPP pole k_{xp}.

polaritons to travel long distances. Lalanne and Hugonin [7] explained the experimental results by suggesting that silver oxidizes producing a silver sulfide tarnish layer when the silver is in contact with air, and that this tarnish would bring their results more in line with experiment. In a follow up comment, Gay *et al*. [8] stated that further numerical and experimental studies indicate that after a short distance from the aperture it does indeed appear that surface plasmons are the dominant mode of propagation, although interpretation of the near aperture field response was left open.

In this paper we extend the analysis of Lalanne and Hugonin [7] by further dissecting the fields along the interface, both in proximity to and at distances away from the source, in order to determine the relative contributions of various parts of this complex wave.

II. Analysis

As in [7], in this discussion the excitation of the surface wave is accomplished by placing a 2-D magnetic line current along the y-axis perpendicular to the page, shown in Fig. 2. The line source lies on the interface between air and silver, with the z-direction perpendicular to the interface. This arrangement gives rise to a TM field structure, which has three non-zero electromagnetic field components H_y, E_x, and E_z. A straightforward analysis that can be found in many textbooks and technical papers, e.g. [9], yields the magnetic field

$$H_y(x) = -\frac{k_o}{2\pi\eta_o}\int_{-\infty}^{\infty}\tilde{G}(k_x)e^{-jk_x x}dk_x \tag{1}$$

$$\tilde{G}(k_x) = \frac{1}{\tilde{D}(k_x)},\ \tilde{D}(k_x) = \frac{k_{z2}}{\varepsilon_2} + \frac{k_{z1}}{\varepsilon_1} \tag{2}$$

$$k_{z1,2} = \sqrt{k_{1,2}^2 - k_x^2} \tag{3}$$

where $\tilde{G}(k_x)$ is the Green function in terms of the spectral variable k_x, ε_1 is the dielectric constant of the upper half-space and ε_2, containing a negative real part, is the dielectric constant of the silver lower half-space. Assuming the permeability of the two regions are the same as that of free space, the location of the surface wave pole k_{xp}, which can be found analytically by setting $\tilde{D}(k_x)$ to zero, is

$$k_{xp} = k_o\sqrt{\frac{\varepsilon_1\varepsilon_2}{\varepsilon_1+\varepsilon_2}} \tag{4}$$

and the corresponding residue is

$$R_p = \frac{1}{\tilde{D}'(k_{xp})},\ \tilde{D}'(k_x) = -k_x\left(\frac{1}{\varepsilon_2 k_{z2}} + \frac{1}{\varepsilon_1 k_{z1}}\right). \tag{5}$$

Note that, for later convenience, we have not included the term $\exp(-jk_{xp}x)$ in the residue definition.

The spectral domain Green function $\tilde{G}(k_x)$ has branch points at k_1 and k_2, the wave numbers of air and silver respectively. Air is lossless, so k_1 is real and therefore lies on the real axis, as shown in Fig. 3, whereas silver has significant loss, so k_2 is far removed from the real axis. The field can be obtained by integrating in the k_x-plane along the real axis from minus to plus infinity by means of the definitions $\mathrm{Im}(k_{z1}) < 0$ and $\mathrm{Im}(k_{z2}) < 0$ on the top sheet of the complex plane for both branch cuts. The tedious numerical integration out to infinity on the real axis can be considerably improved upon by adjusting the integration path so that the integrand of (1) decays rapidly. The integration contour is therefore deformed down vertically [10]–[13], so that the original integration path is replaced by C_1, a path that passes from infinity on the lower Riemann sheet defined by the Sommerfeld branch cut around the k_1 branch point and back down to infinity on the upper sheet. At infinity the path is again vertical and passes around the second branch point k_2 and back down to infinity on the upper sheet of the k_1 and k_2 branch points. An important consequence of this arrangement is the position of the pole k_{xp} relative to the integration path as discussed below.

The contribution from the integral around the branch point at k_2 is negligible because, as can be seen in Fig. 3, the branch point lies well below the real axis so exponential decay due to the imaginary part of k_x is significant. Integration along the path around k_1 produces a field Lalanne and Hugonin [7] referred to as the creeping wave. It will be shown shortly that the term 'creeping wave' is not a single physical wave but rather in this context it is used to refer to a combination of two other types of waves. Integration around the k_{xp} pole produces a $-2\pi j$ residue given in (5) - minus because integration is in the negative sense direction around this pole - which accounts for the SPP wave. The spatial domain Green function can now be expressed in

terms of its pole and branch point components as,

$$G(x) = \underbrace{\int_{C_1} \tilde{G}(k_x) e^{-jk_x x} dk_x}_{\text{CreepingWave}} + \underbrace{\int_{C_2} \tilde{G}(k_x) e^{-jk_x x} dk_x}_{\text{Negligible}} - \underbrace{2\pi j R_p e^{-jk_{xp} x}}_{\text{SPPWave}}. \quad (6)$$

Given the foregoing analysis, we now investigate the behavior and relative strengths of the creeping wave and SPP wave.

Depending on the wavelength of the incident wave, the pole k_{xp} can be very close to the branch point k_1. It is important to note that this SPP pole lies to the right of the integration path C_1, which means that it is captured in the contour deformation process and therefore represents a wave. This location is consistent with the dielectric constant of silver, which has a negative real part at the optical frequencies considered. If the real part of the dielectric constant is positive, this pole will lie to the left of the integration path and is therefore not explicitly captured in the contour deformation. In that case one would say that there is no SPP wave but rather what is referred to as a Zenneck wave in the low frequency literature. The SPP pole therefore occurs in two distinct physical states: It exists as a plasmon wave when the real part of ε_2 is negative, as is the case in noble metals below plasma resonance frequency, and it exists when the real part of ε_2 is positive, but then the pole is not captured and it has long been a question as to whether it is an actual wave. Rather than following the Sommerfeld branch cuts whereby the pole is captured in both of these cases, the vertical integration path, C_1 in Fig. 3, more closely follows the physics associated with the pole. The pole passes across the vertical integration path from the left side Zenneck region to the right side surface plasmon region, where it is captured by the integration path coincident with the change of the real part of the substrate dielectric constant from positive to negative.

The controversy involving the question as to whether a Zenneck pole actually yields a wave has enjoyed a rich history since it was first found to be consistent with Maxwell's equations by Zenneck [14] in 1907 and was later quantified by Sommerfeld [15] in 1909. However Collin in his 2004 paper [16] presented a detailed study of historical work on this subject along with mathematical evidence that the complex plane pole in question is not captured by the integration path and therefore a Zenneck wave is not launched when the real part of ε_2 is positive. His argument centers on demonstrating that in a complex saddle point integration plane the steepest descent path bypasses the Zenneck pole at all observation angles unless the real part of ε_2 is negative, in which case the pole is captured and therefore a wave, in this case a surface plasmon wave, is launched. However for an ε_2 with a positive real part, at angles very close to the interface of the two material regions, the Zenneck pole can influence the field even though no Zenneck wave actually exists. The observations above, and the fact that the vertical integration path below the k_1 branch point is the steepest descent path in the k_x-plane, parallel the conclusions made by Collin. Similar arguments can be made if the contribution due to the C_1 path is analyzed using the s-plane integration technique described below.

TABLE I
THE k_x - PLANE SURFACE PLASMON POLARITON POLE AND CREEPING WAVE BRANCH POINT PROXIMITY $|k_{xp} - k_1|$ AND POLE RESIDUE $|R_p|$ VERSUS WAVELENGTH

λ_0 [nm]	$\lvert k_{xp} - k_1 \rvert$	$\lvert R_p \rvert$
633	3.292×10^{-2}	2.514×10^{-1}
852	1.560×10^{-2}	1.748×10^{-1}
3000	1.506×10^{-3}	5.481×10^{-2}
9000	1.908×10^{-4}	1.953×10^{-2}

The Lezec and Thio experiment [5] was carried out in silver at 850 nm. In the case of bulk silver at this wavelength the real part of the dielectric constant is negative and the imaginary part, which represents loss is also negative. The surface plasmon pole is therefore in a position in the complex k_x-plane which will allow it to be captured by the integration path described above. As such, this pole can be legitimately described as representing a wave.

Table I shows the k_x-plane distance between the surface plasmon polariton pole k_{xp} and the branch point k_1 (normalized to k_o) and the corresponding pole residue at several wavelengths of interest. Notice that as wavelength increases, the plasmon pole approaches the branch point, and the residue decreases, indicating that the strength of the SPP wave is significantly lessened at longer wavelengths where the conductivity of silver begins to markedly increase. The real and imaginary parts of the dielectric function of bulk silver in the optical range were obtained using measurement data [17] subjected to a partial fraction fit [18].

We next turn attention to the creeping wave, which is due to the integral over the contour C_1. In order to evaluate the contour integral around the branch point, it is useful to transform from the k_x-plane to the s-plane as,

$$k_x = k_1 - js^2, \; s = e^{j\pi/4}\sqrt{k_x - k_1}. \quad (7)$$

The integrands on the left and right hand side of the k_x-plane branch cut are combined to form a single s-plane argument. Integration is from zero to infinity along the s-plane real axis giving the simplified result,

$$\text{Creeping wave} = -2je^{-jk_1 x} \int_0^\infty \tilde{F}(s) e^{-xs^2} s \, ds \quad (8)$$

$$\tilde{F}(s) \equiv \tilde{G}^+(s) - \tilde{G}^-(s)) = \frac{-2\left(\frac{k_{z1}}{\varepsilon_1}\right)}{\left(\frac{k_{z2}}{\varepsilon_2}\right)^2 - \left(\frac{k_{z1}}{\varepsilon_1}\right)^2} \quad (9)$$

$$k_{z1} = -s\sqrt{2jk_1 + s^2} \quad (10)$$

where $\tilde{G}^{\pm}(s) = \tilde{G}(k_x = k_1 - js^2)$ is evaluated on the positive and negative real axis sides of C_1. The s-plane, including the

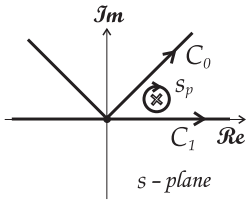

Fig. 4. Complex s-plane showing real axis integration path and surface plasmon pole position.

SPP pole and the integration path again indicated as C_1, is shown in Fig. 4. The real axis path in the s-plane passes very close to the SPP pole. Notice that the imaginary part of the SPP pole is positive whereas a Zenneck pole would lie below the s-plane real axis. The location of the SPP pole affects the manner in which the creeping wave integral is evaluated. The branch point at k_1 corresponds to $s = 0$ in the s-plane. Observe that near the branch point, which is the s-plane origin, $\tilde{F}(s)$ is proportional to s because k_{z1} is proportional to s. Also $\tilde{F}(s)$ has a SPP pole s_p, which is near the origin. The creeping wave integral is most efficiently evaluated by subtracting and adding the SPP pole in the creeping wave integrand,

$$I_1 = \int_0^\infty \tilde{F}(s) e^{-xs^2}\, s\, ds. \\ = \int_0^\infty \left[\tilde{F}(s) - \frac{B_p s}{s^2 - s_p^2}\right] e^{-xs^2}\, s\, ds + \frac{B_p}{2} \underbrace{\int_{-\infty}^{\infty} \frac{e^{-xs^2}}{s^2 - s_p^2} s^2 ds}_{I_p}. \tag{11}$$

The coefficient B_p is related to the residue according to $B_p = jR_p/s_p$, where R_p is easily calculated and given in (5) above. Most of the contribution to the first integral in (11) comes from the region near the origin, although the now dominant term $s^2 \exp(-xs^2)$, where x and s are positive, decreases rapidly as $s \to 0$. Although well behaved, it turns out that the contribution due to this term, which must be evaluated numerically, is almost negligible in value compared to the second integral, which is the SPP pole contribution that has been added back. An illustration of the amplitude difference between the two is shown for $\lambda_o = 9000$ nm in Fig. 5. In Fig. 5(a) the real and imaginary parts of the original integrand in the visible region are plotted five free space wavelengths along the interface away from the line source. At this wavelength, the pole has moved close to the branch point producing a rapid spatial variation in the integrand near the origin in the s-plane. As presented in (11) the pole is then subtracted and the new integrand, shown in Fig. 5(b), is about three orders of magnitude smaller, better behaved, and it is easy to integrate, although the result is negligible compared to the dominant behavior of the pole. After one wavelength the value of this integral, the first term on the right hand side of (11), is a constant two orders of magnitude below the total creeping wave contribution, the solid line in Fig. 6.

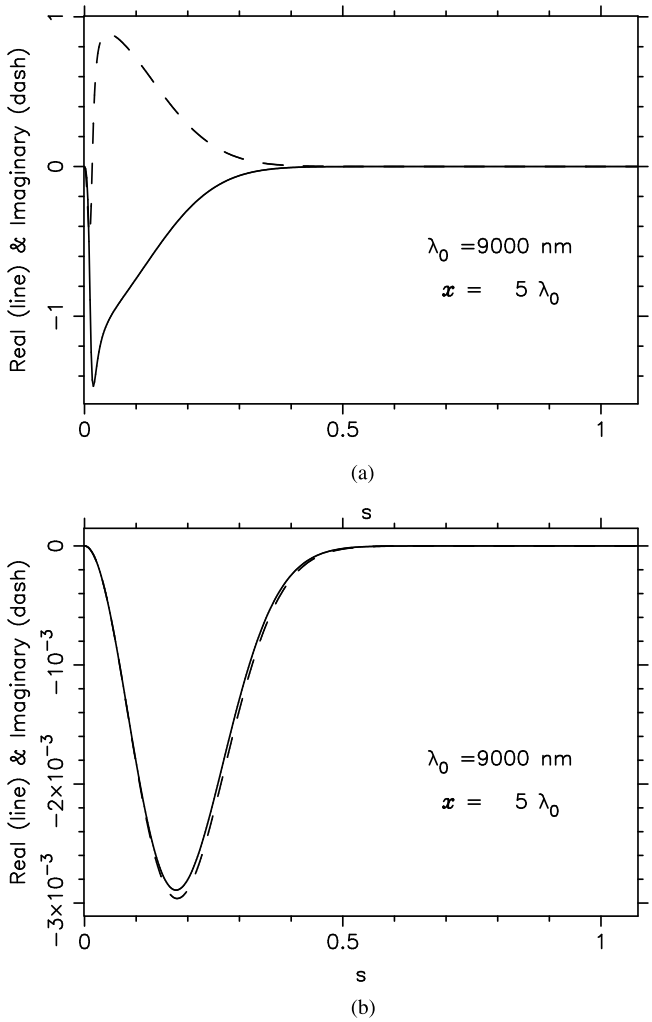

Fig. 5. The creeping wave integrand in the far infrared region before (a), and after (b), the surface plasmon pole has been subtracted.

The second integral in (11), I_p, can be analytically evaluated,

$$I_p(x) = \sqrt{\frac{\pi}{x}}[1 + js_p\sqrt{\pi x}\, w(s_p\sqrt{x})] \\ w(\xi) = e^{-\xi^2} erfc(-j\xi). \tag{12}$$

Because the Faddeeva function $w(\cdot)$ has been extensively studied [20], its properties including large and small argument forms are readily available. If the SPP pole (s_p) is near the branch point, which is at the origin, and the distance x from the source is not large, then $\left|s_p^2 x\right| \to 0$ and the second term in brackets in (12) approaches zero. On the other hand, if $\left|s_p^2 x\right| \to \infty$, the asymptotic behavior of the bracketed term for a SPP pole $(\mathrm{Im}(s_p) > 0)$ is

$$1 + js_p\sqrt{\pi x}\, w(s_p\sqrt{x}) \sim -\frac{1}{2s_p^2 x}. \tag{13}$$

From this analysis it is seen that, not far from the source, the behavior is $x^{-1/2}$ and farther away $x^{-3/2}$, so that

$$I_p(x) \sim \begin{cases} x^{-1/2} & \text{for small and moderate distance } x \\ x^{-3/2} & \text{for sufficiently large distance } x. \end{cases} \tag{14}$$

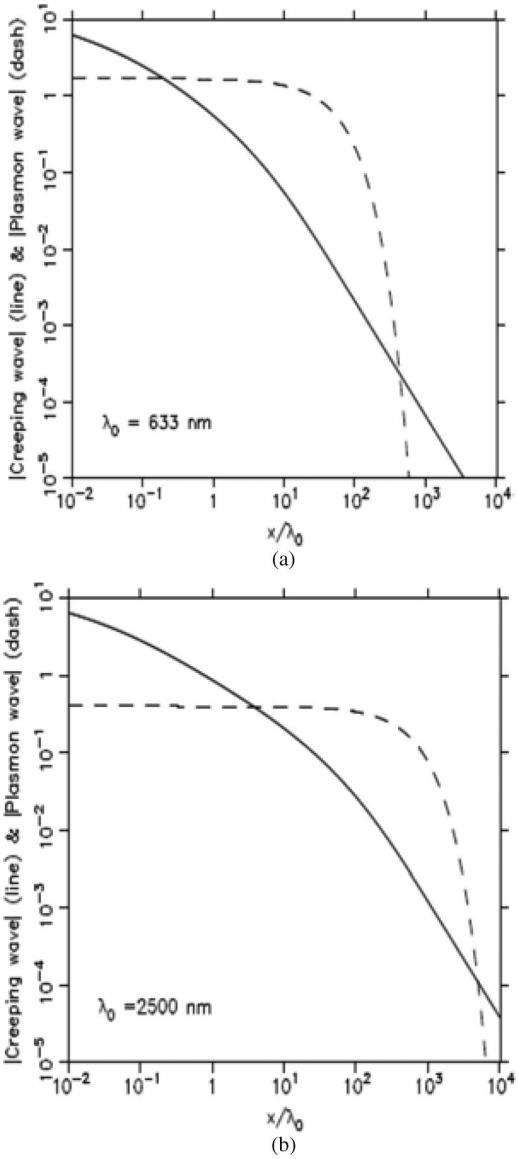

Fig. 6. Logarithmic scale comparison of creeping wave and surface plasmon polariton wave normalized amplitude for bulk untarnished silver as a function of distance from the source at (a) 633 nm (b) 2500 nm.

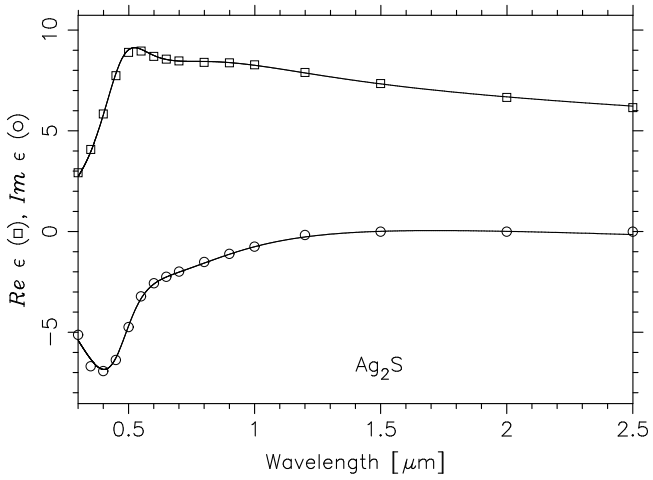

Fig. 7. Partial fraction fit (solid line) for measured real and imaginary parts of the dielectric function of silver sulfide.

The $x^{-3/2}$ result is similar to the behavior of the so called lateral or Norton wave. This is what Lalanne and Hugonin [7] observed and referred to as a creeping wave.

The behavior of the creeping and plasmon waves as a function of distance from the source and normalized by free space wavelength in bulk untarnished silver is illustrated in Fig. 6. The first plot Fig. 6(a) in the visible range at 633 nm and the second Fig. 6(b) at 2500 nm in the short-wavelength infrared, agree with results reported by Lalanne and Hugonin [7]. The amplitude and distance scales in each figure are logarithmic. The solid line is the magnitude of the creeping wave originating from the branch cut integral C_1 in (6). On the same scale is plotted the magnitude of the plasmon wave, the residue with the exponential term in (6). Notice that in Fig. 6(a), at about 1 wavelength the two waves are comparable, so initially near the source the creeping wave dominates but immediately falls below the SPP wave. Because of its small attenuation, the surface plasmon polariton lasts a long distance, but eventually begins to rapidly decay. The creeping wave has an asymptote with a slope $x^{-1/2}$ and a transition region after which the asymptote changes to $x^{-3/2}$, confirming the analysis above. The imaginary part of the dielectric constant, which accounts for loss, is very small for untarnished silver. This allows the surface plasmon to travel almost 100 wavelengths before experiencing significant amplitude decay.

The above analysis was again carried out with an extra 11 nm layer of silver sulfide (Ag2S), which is the tarnish Lalanne and Hugonin suspected might have led to the results in the experiment of Lezec *et al.* Fig. 7 shows tabulated data for the real and imaginary parts of the silver sulphide dielectric function obtained from tabulated measured data [19] together with a partial fraction fit [18]. At 850 nm, the wavelength at which Lezec and Thio performed their experiment [5], the real part of the dielectric constant is negative in the case of bulk silver and positive for silver sulphide. As shown in Fig. 8 for the visible and short-wavelength infrared bands, the creeping wave has a significant amplitude only in a very narrow range near the source. While the SPP wave dominates at distances far away from the source, the additional loss introduced by the tarnish layer only reduces the surface wave travel distance, otherwise it has little effect on the field structure on the boundary.

A parameter study determining the trajectory of the surface plasmon pole as a function of thickness of the sulfide layer, as it is increased from zero to 12 nm in 1 nm increments, is shown in Fig. 9. This shows that no new surface waves are introduced by the tarnish layer, however the downward trajectory of the pole indicates that the power loss will increase with tarnish layer thickness. At shorter wavelengths the complex part of the pole has a steep negative trend as the thickness increases causing the surface plasmon travel distance to significantly shorten. The real part of the surface plasmon pole remains negative regardless of the sulfide layer thicknesses, so it is always captured by the

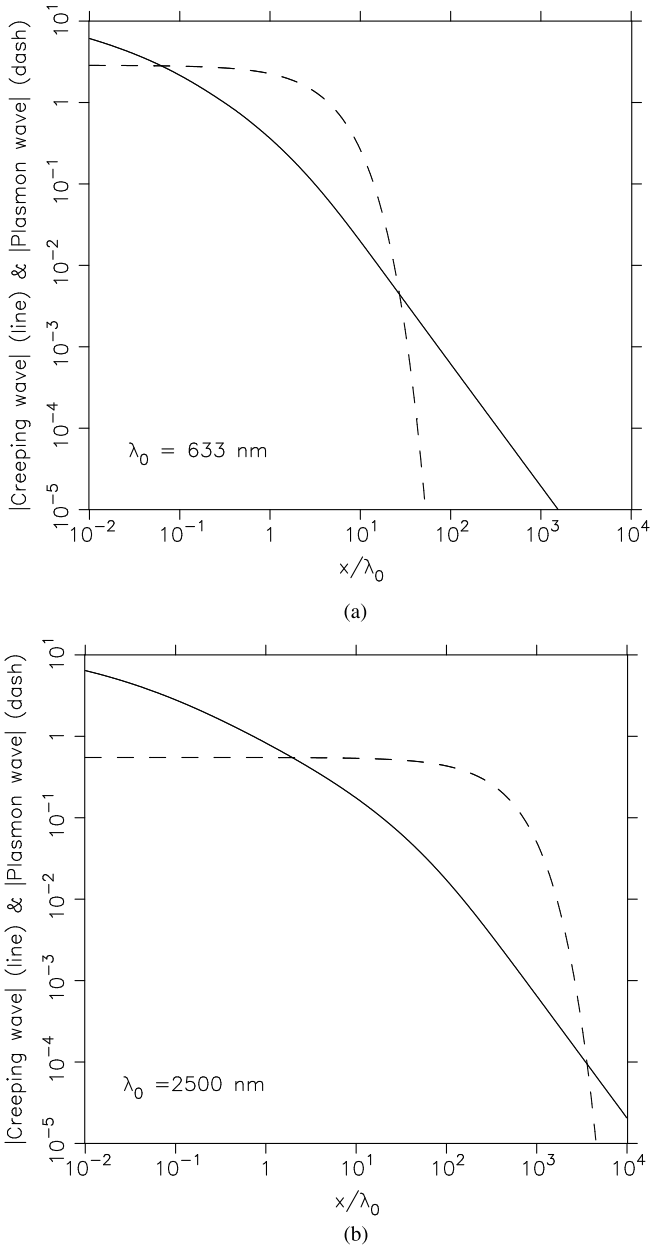

Fig. 8. Logarithmic scale comparison of creeping wave and surface plasmon polariton wave normalized amplitude for an 11 nm silver sulfide adlayer as a function of distance from the source at (a) 633 nm and (b) 2500 nm.

integration contour, thereby remaining a propagating wave with or without the tarnish layer.

Observe that the creeping wave starts at the same amplitude at each frequency in both Figs. 6 and 8. In two-dimensional free space the direct cylindrical wave from a source, often referred to as the space wave, can be expressed as a Hankel function, which has a $x^{-1/2}$ decay behavior, the form shown to occur for small to moderate distance from the source in the analysis above. Although the dielectric function changes with wavelength, it appears that close to the source the creeping wave does not depend on the material properties of the metal; instead, it has the characteristics of a space wave. Also observe that at very long

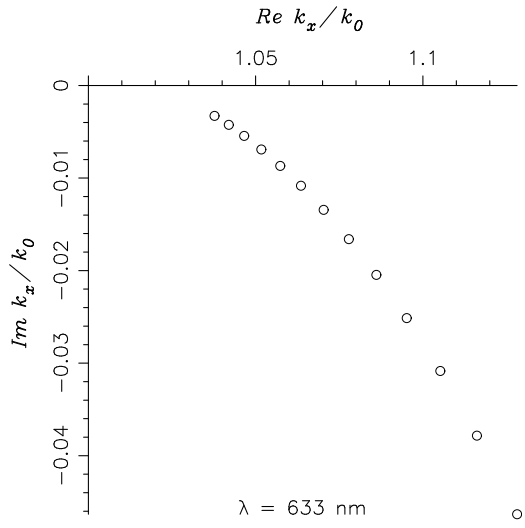

Fig. 9. Pole migration showing the effect of a silver sulfide (Ag_2S) layer on the surface of a silver bar as the Ag_2S layer thickness *d* is increased from 0 to 12 nm in 1 nm increments. The first circle on the left is the zero thickness pole.

wavelengths, such as 2500 nm shown in Fig. 8(b), the plasmon wave is much weaker and the space wave dominates for up to 100 wavelengths, a condition consistent with a magnetic line source lying on a perfect conductor.

III. Conclusion

To conclude, our analysis shows that under one wavelength distance from the source the creeping wave is nearly independent of the metal properties. This is consistent with the line source power contribution due to the direct wave not being affected by the metal. For longer wavelengths, the conductivity of metal increases and the plasmon contribution decreases, due to damping caused by its exponential term. At visible wavelengths the plasmon surface wave contribution dominates even at short distances from the source and in the near-infrared at distances as far as 100 wavelengths. In the intermediate to far infrared wavelengths, plasmon generation is weak.

In each case the creeping wave first scales as $x^{-1/2}$, the same as for a line source in free space, and at large distances as $x^{-3/2}$, which is typical of lateral wave behavior. At distances on the order of a wavelength from the source, the plasmon contribution and creeping wave contributions are therefore approximately the same so neither one dominates. Our analysis confirms the findings of Lalanne and Hugonin [7], that for visible and near-infrared wavelengths the electromagnetic interaction is mainly between the plasmon polariton wave supplemented at distances on the order of a wavelength by a space wave with $x^{-1/2}$ damping. The addition of a silver sulfide tarnish layer only reduces the surface plasmon travel distance and no new guided wave modes appear. Although our calculations show the origin of a two-step process as suggested by Gay *et al.* [6], we have found no evidence in this analysis of the $1/x$ damping in the vicinity of the aperture, as put forward by Lezec and Thio and supported by the measurements of Gay *et al.* It therefore seems likely that

there is indeed an evanescent wave component directly above the aperture which of course is not accounted for by a line source model.

ACKNOWLEDGMENT

The authors express their appreciation to Hasan Tahir Abbas for his assistance in the computations shown of Fig. 1.

REFERENCES

[1] T. W. Ebbesen, H. J. Lezec, H. F. Ghaemi, T. Thio, and P. A. Wolff, "Extraordinary optical transmission through sub-wavelength hole arrays," *Nature*, vol. 391, no. 6668, pp. 667–669, 1998.
[2] H. A. Bethe, "Theory of diffraction by small holes," *Phys. Rev.*, vol. 66, no. 7–8, pp. 163–182, 1944.
[3] C. J. Bouwkamp, "On Bethe's theory of diffraction by small holes," *Philips Res. Rep.*, vol. 5, no. 5, pp. 321–332, 1950.
[4] C. J. Bouwkamp, "Diffraction Theory," *Rep. Prog. Phys.*, vol. 17, no. 1, pp. 35–100, 1954.
[5] H. J. Lezec and T. Thio, "Diffracted evanescent wave model for enhanced and suppressed optical transmission through sub-wavelength hole arrays," *Opt. Exp.*, vol. 12, no. 16, pp. 3629–3651, 2004.
[6] G. Gay, O. Alloschery, B. Viaris de Lesegno, C. O'Dwyer, J. Weiner, and H. J. Lezec, "The optical response of nanostructured surfaces and the composite diffracted evanescent wave model," *Nature Phys*., vol. 2, no. 4, pp. 262–267, 2006.
[7] P. Lalanne and J. P. Hugonin, "Interaction between optical nano-objects at metallo-dielectric interfaces," *Nature Phys.*, vol. 2, no. 8, pp. 551–556, 2006.
[8] G. Gay, O. Alloschery, J. Weiner, H. J. Lezec, C. O'Dwyer, M. Sukharev, and T. Seideman, "The response of nanostructured surfaces in the near-field," *Nature Phys.*, vol. 2, no. 12, p. 792, 2006.
[9] A. L. Cullen, "The excitation of plane surface waves," *Proc. IEE—Part IV: Institution Monographs*, vol. 101, no. 7, pp. 225–234, Oct. 1954.
[10] L. B. Felsen and N. Marcuvitz, *Radiation and Scattering of Waves*. Englewood Cliffs, NJ, USA: Prentice Hall, 1973.
[11] G. D. Bernard and A. Ishimaru, "On complex waves," *Proc. IEE*, vol. 114, no. 1, pp. 43–49, Jan. 1967.
[12] P. Baccarelli, P. Burghignoni, F. Frezza, A. Galli, G. Lovat, and D. R. Jackson, "Uniform analytical representation of the continuous spectrum excited by dipole sources in a multilayer dielectric structure through weighted cylindrical leaky waves," *IEEE Trans. Antennas Propag.*, vol. 52, no. 3, pp. 653–665, Mar. 2004.
[13] K. A. Michalski, "On the efficient evaluation of integrals arising in the Sommerfeld half space problem," in *Moment Methods in Antennas and Scatterers*, R. C. Hansen, Ed. Boston, MA, USA: Artech House, 1990, pp. 325–331.
[14] J. Zenenck, "Über die Fortpflanzung ebener elektromagnetischer Wellen längs einer ebenen Leiterfläche und ihre Beziehung zur drahtlosen Telegraphie," *Ann. Physik*, vol. 328, pp. 846–866, 1907.
[15] A. Sommerfeld, "Über die Ausbreitung der Wellen in der drahtlosen Telegraphie," *Ann. Physik*, vol. 333, no. 4, pp. 665–736, 1909.
[16] R. E. Collin, "Hertzian dipole radiating over a lossy earth or sea: Some early and late 20th-century controversies," *IEEE Antennas Propag. Mag.*, vol. 46, no. 2, pp. 64–79, Apr. 2004.
[17] D. W. Lynch and W. R. Hunter, "Comments on the optical constants of metals and an introduction to the data for several metals," in *Handbook of Optical Constants of Solids*, E. D. Palik, Ed. San Diego, CA, USA: Academic, 1998, pp. 275–316.
[18] K. A. Michalski, "On the low order partial fraction fitting of dielectric functions at optical wavelengths," *IEEE Trans. Antennas Propag.*, vol. 61, no. 12, pp. 6128–6135, Dec. 2013.
[19] J. M. Bennett, J. L. Stanford, and E. J. Ashley, "Optical constants of silver sulfide tarnish films," *J. Opt. Soc. Amer.*, vol. 60, no. 2, pp. 224–232, 1970.
[20] G. P. M. Poppe and C. M. J. Wijers, "More efficient computation of the complex error function," *ACM Trans. Math. Softw.*, vol. 16, no. 1, pp. 38–46, 1990.

Robert D. Nevels (M'77–SM'86–F'07–LF'12) received the B.S.E.E. degree from the University of Kentucky, Lexington, KY, USA, the M.S.E.E. degree from Georgia Tech, Atlanta, GA, USA, and the Ph.D. degree from the University of Mississippi, Oxford, MS, USA. He is currently a Professor in electrical engineering at Texas A&M University, College Station, TX, USA. In 1992, he was a Visiting Professor with the Physics Department Institute for Light Sources, Fudan University, Shanghai, China. He served as an Editor of the book *Microwave and Optical Components* in 1992 and 2003. He was the General Chairman of the 2002 IEEE Antennas and Propagation Symposium and the IEEE AP-S Society President in 2010. His current research interests include analytical and numerical methods in electromagnetics and antennas on material surfaces.

Krzysztof A. Michalski (S'78–M'81–SM'88–F'01) received the M.S. degree from the Wrocław Technological University, Wrocław, Poland, in 1974, and the Ph.D. degree from the University of Kentucky, Lexington, KY, USA, in 1981, both in electrical engineering. From 1982 to 1986, he was with the University of Mississippi, and since 1987, he has been with Texas A&M University, College Station, TX, USA. He has also held visiting professorships with Ecole Polytechnique Fédérale de Lausanne, Université de Nice—Sophia Antipolis, Universitat Politecnica de Catalunya, and Technische Universität München, and served as a Visiting Scientist at Sandia Laboratories and the National Institute of Standards and Technology. His research interests include electromagnetic theory and computational electromagnetics, with emphasis on Green function methods and layered media.